

---

# Low-Light Video Enhancement via Spatial-Temporal Consistent Illumination and Reflection Decomposition

---

Xiaogang Xu<sup>1,2</sup> Kun Zhou<sup>3</sup> Tao Hu<sup>4</sup> Ruixing Wang<sup>5</sup> Hujun Bao<sup>2</sup>

<sup>1</sup> The Chinese University of Hong Kong <sup>2</sup> Zhejiang University

<sup>3</sup> The Chinese University of Hong Kong (Shenzhen) <sup>4</sup> National University of Singapore

<sup>5</sup> Honor Device Co., Ltd.

xiaogangxu00@gmail.com

## Abstract

Low-Light Video Enhancement (LLVE) seeks to restore dynamic and static scenes plagued by severe invisibility and noise. One critical aspect is formulating a consistency constraint specifically for temporal-spatial illumination and appearance enhanced versions, a dimension overlooked in existing methods. In this paper, we present an innovative video Retinex-based decomposition strategy that operates without the need for explicit supervision to delineate illumination and reflectance components. We leverage dynamic cross-frame correspondences for intrinsic appearance and enforce a scene-level continuity constraint on the illumination field to yield satisfactory consistent decomposition results. To further ensure consistent decomposition, we introduce a dual-structure enhancement network featuring a novel cross-frame interaction mechanism. This mechanism can seamlessly integrate with encoder-decoder single-frame networks, incurring minimal additional parameter costs. By supervising different frames simultaneously, this network encourages them to exhibit matching decomposition features, thus achieving the desired temporal propagation. Extensive experiments are conducted on widely recognized LLVE benchmarks, covering diverse scenarios. Our framework consistently outperforms existing methods, establishing a new state-of-the-art (SOTA) performance.

## 1 Introduction

Low-light enhancement aims to enhance underexposed images and videos captured in low-light conditions Xu et al. [2022], Wang et al. [2021a], improving their visual quality while reducing noise. This is a longstanding and important topic in computer vision, with wide-ranging applications, such as improving portrait photography on mobile devices Ignatov et al. [2017], Hasinoff et al. [2016] and supporting various downstream tasks, including nighttime face recognition Ma et al. [2022], Wang et al. [2022a] and vehicle detection Fu et al. [2023a], Wu et al. [2022b].

Numerous methods have been proposed to enhance underexposed images using supervised learning Wang et al. [2021b], Xu et al. [2022, 2023b], Cai et al. [2023], Wang et al. [2022b], yielding impressive results. However, these methods still struggle to provide satisfactory performance when applied to videos, a popular media format. The key challenge when enhancing videos is the need for consistent enhancement results across corresponding locations in different frames, which vary both spatially and temporally. Current methods rely on paired training data, where the ground truth ensures this consistency. Unfortunately, there is a scarcity of real-world, high-quality, spatially aligned video pairs for dynamic scenes, resulting in limited generalization capabilities for unseen videos with varying conditions.

One solution is to incorporate parameterized enhancement models with physical significance into the enhancement process, reducing the reliance on training data, e.g., Retinex theory Land [1977].

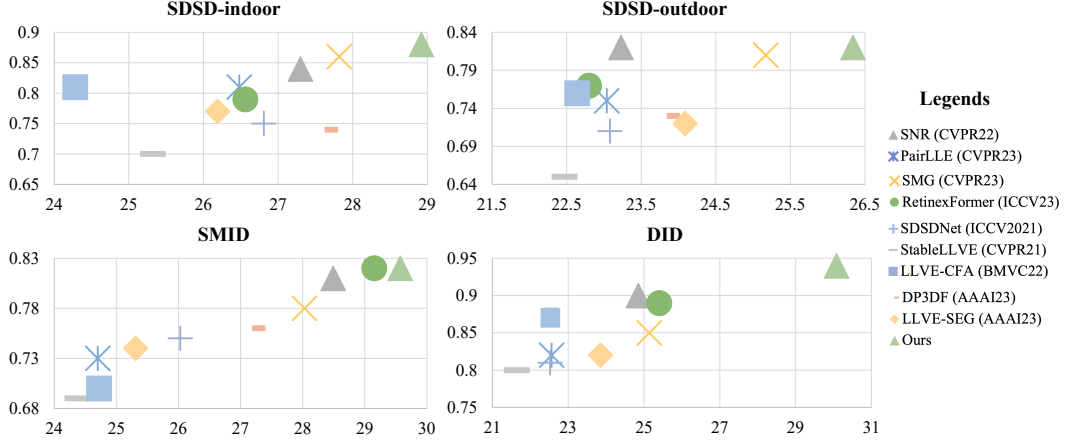


Figure 1: Our method *consistently* achieves SOTA performance on *different LLVE datasets* with the same network architecture.

According to this theory, an observed image  $I$  can be decomposed into its illumination component  $L$  and reflectance component  $R$  using the equation  $I = L \otimes R$ , where  $\otimes$  denotes element-wise multiplication. Several approaches Zhang et al. [2019], Wu et al. [2022a], Fu et al. [2023b] have been developed to predict both  $R$  and  $L$  under normal illumination conditions for a low-light input image. However, a suitable strategy for obtaining the Retinex decomposition in normal-light conditions for low-light input videos is currently lacking. Ensuring both temporal and spatial consistency in decomposition is crucial, yet previous strategies were primarily designed for individual images, thus posing a challenge for video processing.

In this paper, we introduce an innovative approach to attain a consistent Retinex decomposition for normal-light video outputs, ensuring consistency in both spatial and temporal dimensions. We leverage cross-frame correspondences and real-world physical continuity constraints to achieve this decomposition without the need for explicit supervision. Furthermore, to enhance the consistency of the decomposition, we’ve developed an efficient dual-structure enhancement network featuring a novel cross-frame interaction mechanism.

Differing from some previous methods Wang et al. [2019a, 2021a], which directly assume the reflection term as the enhanced version, our approach follows Cai et al. [2017], Wei et al. [2018], Wu et al. [2022a], Fu et al. [2023b], i.e., aims to *recover both the reflection and illumination components of normal-light images from the provided low-light inputs*. Previous methods have verified that satisfying image-level reflection and illumination decomposition can be achieved with suitable reflection and illumination priors via a data-driven manner. In this paper, we aim to design appropriate priors for video data to implement the decomposition.

We recognize that the reflectance component  $R$  should represent the physical properties of objects, which should remain consistent across various observation perspectives Wei et al. [2018]. To achieve this, we first calculate corresponding locations in videos and utilize these computed spatial-temporal correspondences, along with uncertainty values, to link the reflection terms across different frames. Conversely, the illumination terms are subject to a spatial smoothness loss to model real-world physical constraints Wei et al. [2018]. This approach allows us to establish a consistency constraint specifically for temporal-spatial illumination and appearance in the enhanced videos, without requiring additional supervision information.

Additionally, the architecture of the enhancement networks plays a crucial role in shaping the decomposition results. It is important that different frames share features and receive simultaneous supervision, promoting the alignment of feature representations to synthesize Retinex parameters. In our paper, we introduce a novel dual network structure capable of achieving such feature propagation. Two frames are used as inputs, and their features are shared within the designed Cross-Frame Interaction Module (CFIM). CFIM facilitates interaction through a combination of long-range cross-frame attention computation and short-range channel-spatial fusion, ensuring the accurate and comprehensive merging of features from both global and local perspectives. CFIM can be seamlessly integrated into any encoder-decoder single-image enhancement structure by inserting it at the deepest hidden layer. In this paper, we illustrate this with the simplest U-Net Ronneberger et al. [2015] as an example, and it’s worth noting that CFIM comprises only 0.4M parameters.

We performed experiments on various widely recognized video enhancement datasets Wang et al. [2021a], Chen et al. [2019], Fu et al. [2023a], Zhang et al. [2021]. Our results, both quantitative and qualitative, consistently demonstrate the effectiveness and state-of-the-art (SOTA) performance of our framework, as shown in Fig. 1. Furthermore, we conducted a large-scale user study involving 100 participants, which clearly showcased the superiority of our enhanced results in terms of human subjective perceptions.

In summary, our contributions are three-fold.

- We introduce a novel canonical form for LLVE that predicts spatial-temporal consistent Retinex decomposition for normal-light outputs. This innovative decomposition strategy leverages spatial-temporal correspondences and continuity.
- We design a new LLVE network that facilitates interaction among the features of different frames, leading to a consistent decomposition.
- We conduct extensive experiments on public datasets, illustrating the effectiveness of our proposed framework.

## 2 Related Work

**Low-Light Image Enhancement.** To enhance the quality of a low-light video, image enhancement methods can be applied on a frame-by-frame basis. In recent years, learning-based Low-Light Image Enhancement (LLIE) techniques Yan et al. [2014, 2016], Lore et al. [2017], Cai et al. [2018], Zamir et al. [2020], Xu et al. [2020], Zeng et al. [2020], Kim et al. [2021], Zhao et al. [2021], Zheng et al. [2021], Wang et al. [2021b], Liu et al. [2021], Yang et al. [2021b], Jiang et al. [2021], Yang et al. [2021a] have made significant advancements, with a primary focus on supervised approaches thanks to the abundance of image pairs available for training. Xu et al. [2022] introduced spatial-varying operations, considering Signal-to-Noise Ratio (SNR) as a prior factor. However, when applying image enhancement algorithms to individual frames, the issue of flickering often arises.

**Low-Light Video Enhancement.** In addition to the need for LLIE, there is a growing demand for video enhancement, considering the widespread use of videos as a popular data format on the internet and in photographic equipment. Various approaches have been proposed in this context Chen et al. [2019], Triantafyllidou et al. [2020], Ye et al. [2023], Lv et al. [2023], Xu et al. [2023a], Fu et al. [2023a]. Danai et al. [2020] introduced a data synthesis mechanism to generate dynamic video pairs from SID Chen et al. [2019]. Wang et al. [2021a] proposed a multi-branch network that simultaneously estimates noise and illumination, suitable for videos with severe noise conditions. Liu et al. [2023] and Liang et al. [2023] used prior event information to learn enhancement mapping for brightening videos. Xu et al. [2023a] designed a parametric 3D filter tailored for enhancing and sharpening low-light videos. Recently, Fu et al. [2023a] introduced a video enhancement method called LAN, which iteratively refines illumination and adaptively adjusts it. However, it’s important to note that LAN lacks an explicit constraint for maintaining consistent reflectance and illumination decomposition.

Several datasets for video enhancement, encompassing both static Chen et al. [2019], Jiang and Zheng [2019], Wang et al. [2019b], Triantafyllidou et al. [2020] and dynamic motions Wang et al. [2021a], Fu et al. [2023a], have been introduced. In this paper, we introduce a novel LLVE method, designed to enhance effects on these datasets. Our decomposition method explicitly and consistently models reflectance and illumination for all frames, with the guidance of the videos themselves.

## 3 Method

We commence by revisiting the formulation of the Retinex theory in Sec. 3.1. Following that, we provide a detailed exposition of our decomposition strategy specifically tailored for video data in Sec. 3.2. Subsequently, in Sec. 3.3, we delve into the description of our cross-frame interaction. Finally, the training loss for our framework will be introduced in detail.

### 3.1 Retinex Model

**Retinex Theory.** When presented with an image  $I$  (in this paper, we denote the low-light image as  $I_d$  and the normal-light image as  $I_n$ , with  $d$  and  $n$  serving as subscript abbreviations), we assume its

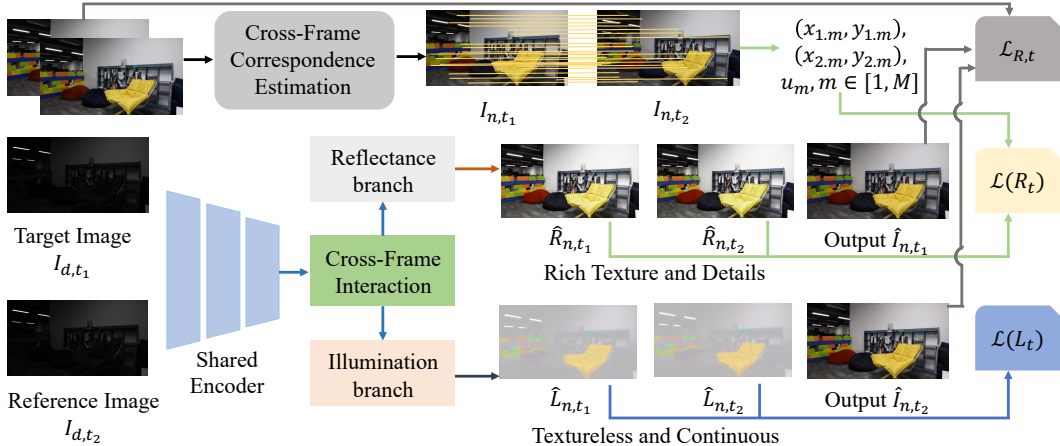


Figure 2: Our framework provides a comprehensive solution that includes explicit and consistent modeling for Retinex decomposition of enhanced normal-light outputs across different frames. To achieve this, we enforce consistent features in the reflectance terms across different frames by leveraging computed correspondences in the temporal dimension of videos ( $\mathcal{L}(R_t)$ ). Simultaneously, we ensure that the illumination terms exhibit a spatially continuous distribution ( $\mathcal{L}(L_t)$ ), aligning with real-world scenarios. Furthermore, our network incorporates cross-frame interaction and simultaneous supervision of different frames within a video, encouraging consistent Retinex features among these frames. For a more detailed visual representation, please refer to Fig. 3.

decomposition into illumination  $L$  and reflectance  $R$  follows the Retinex theory Land and McCann [1971], Fu et al. [2023b], as

$$I = L \otimes R, \quad (1)$$

where  $\otimes$  denotes the element-wise multiplication,  $L$  and  $R$  can be formulated for different channels Wang et al. [2019a], Cai et al. [2023], i.e., the channel number is 3 for the sRGB domain. In this context,  $L$  describes the light intensity of objects, which is expected to exhibit piece-wise continuity. On the other hand,  $R$  represents the physical properties of the objects, encompassing textures and details observed in the data  $I$ . If we obtain  $L$  and  $R$  in the normal-light conditions for a given input low-light image, the target normal-light image can be acquired accordingly. Numerous methods have been proposed to address this decomposition problem Zhang et al. [2019], Wu et al. [2022a], Fu et al. [2023b], and their common objective can be summarized as

$$\mathcal{L} = \|I - L \otimes R\| + \mathcal{L}(L) + \mathcal{L}(R), \quad (2)$$

where  $\mathcal{L}(L)$  and  $\mathcal{L}(R)$  denote the constraints for illumination  $L$  and reflectance  $R$ , respectively.

**Shortcoming of current Retinex models for videos.** Several prior approaches have been devised to attain this desired decomposition by imposing different constraints on the two components, such as structural and smoothness constraints Li et al. [2018], Wei et al. [2018]. Nevertheless, there is a scarcity of satisfactory Retinex decomposition prediction tailored for sequential video data. The issue concerning the decomposition of video data can be summarized as

$$\mathcal{L}_v = \mathbb{E}_{t=1:T}[\mathcal{L}_{R,t} + \mathcal{L}(L_t) + \mathcal{L}(R_t)], \quad \mathcal{L}_{R,t} = \|I_t - L_t \otimes R_t\|, \quad (3)$$

where  $\mathbb{E}$  is the average operation,  $T$  is the number of frame. Compared with Eq. 2, we need to simultaneously guarantee the decomposition quality and the consistency among different frames' results.

**Video data guide Retinex models by themselves.** We have discovered that video data itself can play a crucial role in facilitating the achievement of a satisfactory Retinex decomposition prediction for normal-light outputs, thus obviating the need for external priors typically used in low-light enhancement. By establishing correspondences among different frames, we can impose specific constraints: the reflectance of each frame, denoted as  $R_t$ , should faithfully represent the intrinsic texture of objects within the target scene, remaining consistent regardless of changes in viewpoint. Likewise, the illumination of each frame, denoted as  $L_t$ , should exhibit the desired continuity consistent with real-world physical properties. For further elaboration, please refer to Sec. 3.2.

**Problem formulation.** We adopt the supervised setting. Given a clip of low-light data  $I_{d,t}$ ,  $t \in [1, T]$ , there is a paired normal-light data  $I_{n,t}$ ,  $t \in [1, T]$ . We aim to directly obtain the decomposition of  $I_{n,t}$  from  $I_{d,t}$  using network  $f$ , as

$$\hat{L}_{n,t}, \hat{R}_{n,t} = f(I_{d,t}), \hat{I}_{n,t} = \hat{L}_{n,t} \otimes \hat{R}_{n,t}, \quad (4)$$

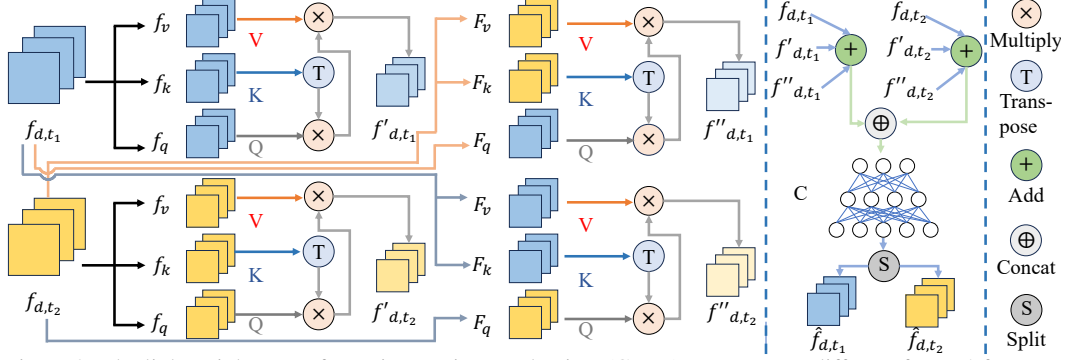


Figure 3: The lightweight cross-frame interaction mechanism (CFIM) to propagate different frames’ features, along with the cross-frame attention and spatial-channel fusion. Cross-frame interaction can be employed in the deep feature space of arbitrary single-image encoder-decoder frameworks, and we choose U-Net here.

where  $\hat{L}_{n,t}$  and  $\hat{R}_{n,t}$  are the estimated targets (several examples are displayed in Fig. 4), and  $\hat{I}_{n,t}$  is the predicted enhancement result.

### 3.2 Spatial-Temporal Consistent Decomposition

**Motivation.** Video can be conceptualized as static/dynamic 3D multi-view data Wang et al. [2023b,a]. Prior research has demonstrated that the multi-view data itself can be harnessed to decompose the view-dependent and view-independent elements, which respectively encapsulate the intrinsic texture and view-altering illuminations Wang et al. [2023a]. Thus, once we establish correspondence relationships among  $I_{d,t}$  for all  $t$ , we can apply the view-independent constraint to derive the reflectance component, denoted as  $\hat{R}_{n,t}$ , as it represents the intrinsic properties of the target scene. Subsequently, obtaining the illumination component, denoted as  $\hat{L}_{n,t}$ , becomes achievable through the utilization of the inherent image reconstruction loss, in conjunction with adherence to the continuity assumption.

**Implementation of correspondences.** Obtaining correspondences for  $I_{d,t}$ ,  $t \in [1, T]$ , can be a challenging task due to the presence of various degradations, including visibility issues and noise. Fortunately, we have access to corresponding normal-light data, which significantly aids in establishing these correspondences, as illustrated in Fig. 2, where  $I_{d,t}$  and  $I_{n,t}$  are pixel-wise aligned.

Given two frames  $I_{n,t_1}$  and  $I_{n,t_2}$ , correspondences can be determined using the prediction network  $F$  Edstedt et al. [2023]. We assume the detection of  $M$  correspondences, denoted as  $c_m = (x_{1,m}, y_{1,m}, x_{2,m}, y_{2,m})$ ,  $m \in [1, M]$ . Each correspondence, represented by  $c_m$ , consists of four coordinates:  $(x_{1,m}, y_{1,m})$  represents the pixel coordinate in  $I_{n,t_1}$ , while  $(x_{2,m}, y_{2,m})$  signifies the coordinate in  $I_{n,t_2}$ . Furthermore, each correspondence is associated with an uncertainty value  $u_m$ , determined through a data-driven approach.

**Constraints formulation.** To satisfy the constraint that the corresponding pixels in the reflectance part are matched, we can formulate  $\mathcal{L}(R_t)$  as

$$\mathcal{L}(R_{t_1,t_2}) = \mathbb{E}_{m \in [1, M]} u_m \|\hat{R}_{n,t_1}[x_{1,m}, y_{1,m}] - \hat{R}_{n,t_2}[x_{2,m}, y_{2,m}]\|. \quad (5)$$

The reconstruction item in Eq. 3 can be denoted as

$$\mathcal{L}_{R,t} = \|I_{n,t} - \hat{L}_{n,t} \otimes \hat{R}_{n,t}\|. \quad (6)$$

Although the illumination part can be obtained via Eqs. 5 and 6, we further incorporate a continuity constraint to align with real-world properties. For a pixel in the video frame, denoted as  $p$ , we introduce a spatial continuity loss on the predicted  $\hat{L}_{n,t}$  as

$$\mathcal{L}(L_t) = \mathbb{E}_t [v_t^p \times [\partial_x \hat{L}_{n,t}(p)]^2 + u_t^p \times [\partial_y \hat{L}_{n,t}(p)]^2], \quad (7)$$

where  $\partial_x$  and  $\partial_y$  are partial derivatives in horizontal and vertical directions, respectively.  $v_t^p$  and  $u_t^q$  are spatially-varying smoothness weights, calculated as

$$v_t^p = (\|\partial_x \mathcal{T}_t(p)\|^{1.2} + \Delta)^{-1}, u_t^q = (\|\partial_y \mathcal{T}_t(p)\|^{1.2} + \Delta)^{-1}, \quad (8)$$

where  $\mathcal{T}_t$  represents the logarithmic transformation of  $I_{d,t}$ , and  $\Delta$  is a small constant (set to 0.0001) used to avoid division by zero. The diagram for the decomposition implementation is shown in Fig. 2.



Figure 4: Visual samples: derive the Retinex decomposition results of enhanced normal-light outputs from the input low-light video data on different datasets.

### 3.3 Dual Network for Consistent Decomposition

**Overview and motivation.** To enhance the consistency of decomposition, it’s crucial for various frames within a video to mutually share features. By incorporating shared features and simultaneous supervisions, the features used for synthesizing Retinex parameters across different frames can exhibit greater consistency. When the video is enhanced frame by frame without feature propagation, the decomposition results tend to be suboptimal due to the inherently challenging nature of maintaining consistency. This observation is empirically validated in our ablation study. Current LLVE methods primarily leverage multiple-frame inputs to facilitate propagation Wang et al. [2021a], Fu et al. [2023a]. However, these strategies come with a notable cost in terms of aligning features, potentially affecting inference efficiency.

In this paper, we introduce an efficient strategy for propagation using a dual approach. This approach entails loading two frames, specifically target frame  $I_{d,t_1}$  and reference frame  $I_{d,t_2}$  (where  $I_{d,t_2}$  can be randomly selected from the temporal neighbors of  $I_{d,t_1}$  during training, and is set as the closest frame of  $I_{d,t_1}$  during inference), propagating features at the deepest layer of the network through our cross-frame interaction (as depicted in Fig. 3), and concurrently supervising these dual outputs to guarantee consistency.

**Feature propagation via long-range attention and short-range fusion in CFIM.** Suppose the feature of  $I_{d,t_1}$  and  $I_{d,t_2}$  are denoted as  $f_{d,t_1}$  and  $f_{d,t_2}$  which is extracted from the same encoder  $E$  in the network  $f$ . To complete the propagation, we initially employ a long-range cross-frame attention operation in the feature space. A traditional attention operation Vaswani et al. [2017] typically consists of the query vector  $q$ , the key vector  $k$ , and the value vector  $v$ . The attention relationship is established using  $A(q, k, v) = \text{softmax}(q \times k^T) \times v$ , where  $\times$  represents matrix multiplication. To enable cross-frame attention, we process the feature via dual paths, as

$$\begin{aligned}\hat{f}_{d,t_1} &= A(f_{d,t_1}, f_{d,t_1}, f_{d,t_1}) + A(f_{d,t_1}, f_{d,t_2}, f_{d,t_2}), \\ \hat{f}_{d,t_2} &= A(f_{d,t_2}, f_{d,t_2}, f_{d,t_2}) + A(f_{d,t_2}, f_{d,t_1}, f_{d,t_1}).\end{aligned}\tag{9}$$

Moreover, a short-range fusion operation is set as the refinement operation to the propagation at both spatial and channel levels. This can be written as

$$\bar{f}_{d,t_1}, \bar{f}_{d,t_2} = S(C(\hat{f}_{d,t_1} \oplus \hat{f}_{d,t_2})),\tag{10}$$

where  $\oplus$  represents channel concatenation,  $C$  refers to the convolution network, and  $S$  signifies channel dimension splitting. The decomposition results for  $I_{d,t_1}$  and  $I_{d,t_2}$  are obtained by processing  $\bar{f}_{d,t_1}$  and  $\bar{f}_{d,t_2}$  through the decoder. We have confirmed that our dual network with synchronous supervision for the outputs of  $I_{d,t_1}$  and  $I_{d,t_2}$  can yield superior decomposition and enhancement results compared to individual enhancement strategies.

### 3.4 Overall Loss Function

During the training, we find it is better to adopt the dual training strategy, i.e., for each  $I_{d,t_1}$ , we sample its neighboring reference  $I_{d,t_2}$  and constrain their outputs simultaneously. Thus, the loss function can be written as

$$\mathcal{L}_v = \mathbb{E}_{t_1, t_2} [\mathcal{L}_{R,t_1} + \mathcal{L}_{R,t_2} + \lambda_1 (\mathcal{L}(L_{t_1}) + \mathcal{L}(L_{t_2})) + \lambda_2 \mathcal{L}(R_{t_1, t_2})],\tag{11}$$

where  $\lambda_1$  and  $\lambda_2$  are the loss weights, and each loss term is defined in Eqs. 5, 6 and 7. Moreover, we observe that the performance of our framework is robust to the choice of the reference frame.

Table 1: Quantitative comparison on SDSO, SMID, and DID datasets. Our method performs the best consistently.

Methods	SDSD-indoor		SDSD-outdoor		SMID		DID	
	PSNR	SSIM	PSNR	SSIM	PSNR	SSIM	PSNR	SSIM
SNR Xu et al. [2022]	27.30	0.84	23.23	0.82	28.49	0.81	24.85	0.90
SMG Xu et al. [2023b]	27.82	0.86	25.17	0.81	28.03	0.78	25.14	0.85
PairLLE Fu et al. [2023b]	23.48	0.71	20.04	0.65	22.70	0.63	22.56	0.82
RetinexFormer Cai et al. [2023]	26.56	0.79	22.80	0.77	29.15	0.82	25.40	0.89
MBLLEN Lv et al. [2018]	22.17	0.66	21.41	0.63	22.67	0.68	24.22	0.86
SMID Chen et al. [2019]	24.84	0.72	23.30	0.67	24.78	0.72	22.28	0.84
SMOJD Jiang and Zheng [2019]	24.63	0.70	22.25	0.68	23.64	0.71	22.13	0.85
SDSDNet Wang et al. [2021a]	26.81	0.75	23.08	0.71	26.03	0.75	22.52	0.81
DP3DF Xu et al. [2023a]	27.63	0.74	23.85	0.73	27.19	0.76	22.39	0.88
StableLLVE Zhang et al. [2021]	25.32	0.70	22.47	0.65	24.37	0.69	21.64	0.80
LLVE-SEG Liu et al. [2023]	26.19	0.77	24.09	0.72	25.31	0.74	23.85	0.82
LLVE-CFA Chhirolya et al. [2022]	24.28	0.81	22.64	0.76	24.72	0.70	22.53	0.87
Ours	<b>28.93</b>	<b>0.88</b>	<b>26.32</b>	<b>0.82</b>	<b>29.60</b>	<b>0.82</b>	<b>30.10</b>	<b>0.93</b>

Table 2: Quantitative comparison on the DAVIS dataset.

Methods	SNR	SMG	PairLLE	RetinexFormer	MBLLEN	SMID
PSNR	20.69	20.18	19.57	21.79	18.63	20.51
SSIM	0.710	0.672	0.667	0.723	0.619	0.686
Methods	SMOJD	SDSDNet	DP3DF	StableLLVE	LLVE-SEG	Ours
PSNR	20.66	21.22	22.04	21.48	21.45	<b>23.38</b>
SSIM	0.697	0.716	0.749	0.732	0.715	<b>0.782</b>

## 4 Experiments

### 4.1 Datasets

Our evaluation is conducted on four publicly available datasets, which encompass a wide range of real-world videos with diverse motion patterns and degradations. (1) SMID Chen et al. [2019]: This dataset consists of static videos with ground truths obtained through long exposure. We followed the procedure provided by SMID, converting the videos from the RAW domain to the sRGB domain using rawpy’s default ISP. (2) SDSO Wang et al. [2021a]: SDSO is a dynamic video dataset collected through electromechanical equipment, including both indoor and outdoor subsets. (3) DID Fu et al. [2023a]: DID is another dynamic video dataset characterized by pronounced camera motion, strict spatial alignment, and diverse scene content. In comparison to SDSO, DID offers more data and is a multi-illumination, multi-camera LLVE dataset. We follow DID’s division into a training set, a test set, and a validation set, maintaining a ratio of 3:1:1. (4) DAVIS Pont-Tuset et al. [2017]: DAVIS is a dataset that includes both scene dynamics and camera motions. To simulate low-light degradation in DAVIS, we followed the methodology outlined in Zhang et al. [2021], further incorporating noise degradation.

### 4.2 Implementation Details

We conducted experiments on all datasets using the same network structure. All modules were trained end-to-end, with the learning rate initialized at  $4e^{-4}$  for all layers, adapted by a cosine learning scheduler. The batch size used was 4. Correspondences were computed using the SOTA method DKM Edstedt et al. [2023]. Additionally, no data augmentation was applied during training. All experiments were executed on a single NVIDIA A100 GPU.

### 4.3 Comparison and Baselines

We conducted a comprehensive comparison with SOTA LLVE methods, including MBLLEN Lv et al. [2018], SMID Chen et al. [2019], SMOJD Jiang and Zheng [2019], SDSONet Wang et al. [2021a], DP3DF Xu et al. [2023a], StableLLVE Zhang et al. [2021], LLVE-SEG Liu et al. [2023], and LLVE-CFA Chhirolya et al. [2022] We also compared our method with SOTA LLIE methods for individual frames, including SNR Xu et al. [2022], SMG Xu et al. [2023b], PairLLE Fu et al. [2023b], RetinexFormer Cai et al. [2023]. All these methods were trained on each dataset using their respective released code and hyper-parameters (e.g., the training epoch that is set to guarantee the convergence). *Note that all these baselines are trained on our unified data split for a fair comparison. The splits slightly differ from those in baselines’ original papers, so the scores of the baselines may vary from the original papers.*

**Quantitative result.** In Table 1, we present the comparative results with the selected baseline methods across the SDSO, SMID, and DID datasets. The table reveals that our approach *consistently*

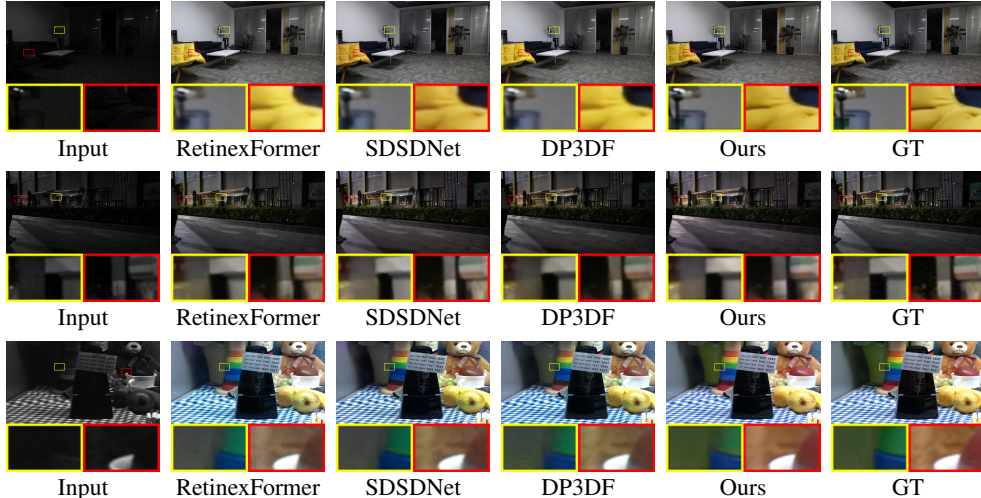


Figure 5: Visual comparisons on SSSD-indoor (top), SSSD-outdoor (middle), and SMID (bottom). The results of our proposed framework, i.e., “Ours”, demonstrate better visual perception with less noise, clearer visibility, and more enhanced details.



Figure 6: Comparisons on DID (top) and DAVIS (bottom). “Ours” has less noise, better visibility and details.

outperforms all other methods, as indicated by the highest PSNR and SSIM scores on all datasets. Notably, our scores exhibit a substantial lead over all others, particularly on DID, which is a large-scale dynamic video dataset. This superiority underscores the robust capability of our method in enhancing real-world videos.

Furthermore, Table 2 provides a summary of the comparative results on DAVIS. In comparison to the degradation synthesis strategy as presented in Zhang et al. [2021], we have extended our approach to include the degradation of a low-light noise term. As a result, our synthesized data encompasses dynamic scenes with pronounced invisibility and perturbations, posing a considerable challenge. As illustrated in Table 2, our method consistently yields the highest PSNR and SSIM values, reaffirming the effectiveness of our approach.

**Qualitative result.** Besides the quantitative comparison, we present visual comparisons with the selected baselines. Fig. 5 showcases the visual comparisons on SSSD and SMID, while Fig. 6 displays visual cases from DID and DAVIS. In general, the results enhanced by our approach exhibit a more natural appearance, including accurate color, well-balanced brightness, enhanced contrast, and precise details without noise. Furthermore, our framework’s results show fewer artifacts in regions with complex textures, and they appear cleaner and sharper compared to the results produced by other methods. This distinction is particularly notable, as most baselines perform well in simpler areas.

#### 4.4 Ablation Study

We assess the critical components of our framework through five ablation cases. (1) “w/o LR” that removes the constraint on learning the reflectance part. (2) “w/o LL” where the constraint on learning the illumination part is removed. (3) “w/o C.F.”: we eliminate the cross-frame attention and fusion in the network, resulting in each frame being enhanced individually. (4) “with M.I.”: This refers to using multiple neighboring frames as input and employing the temporal alignment of deformable

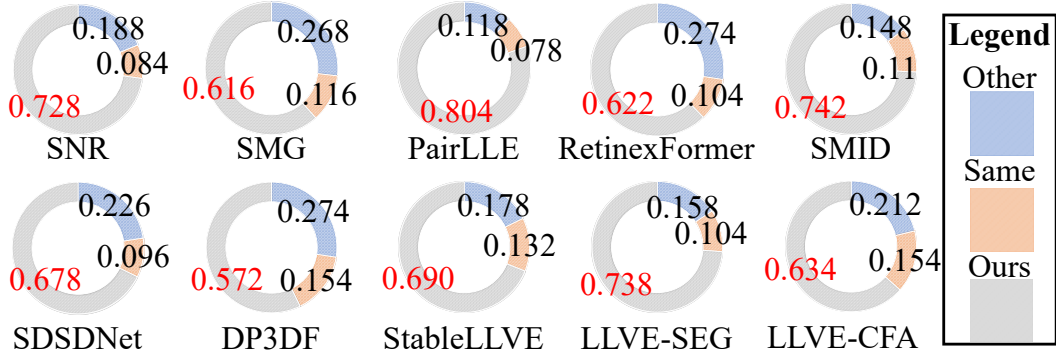


Figure 7: The above pie charts summarize the results of our user study, and ours is preferred by participants.

Table 3: Ablation study on SDDSD, SMID, and DID.

Methods	SDDSD-indoor		SDDSD-outdoor		SMID		DID	
	PSNR	SSIM	PSNR	SSIM	PSNR	SSIM	PSNR	SSIM
w/o LR	25.78	0.77	23.49	0.75	26.37	0.76	27.54	0.86
w/o LL	26.89	0.80	24.19	0.78	27.74	0.79	27.72	0.89
w/o C.F.	25.18	0.82	24.22	0.77	26.75	0.77	25.60	0.85
with M.I.	26.21	0.84	25.36	0.80	28.42	0.79	28.33	0.88
w/o Dual	27.53	0.84	24.83	0.79	27.43	0.78	26.91	0.86
Full	<b>28.93</b>	<b>0.88</b>	<b>26.32</b>	<b>0.82</b>	<b>29.60</b>	<b>0.82</b>	<b>30.10</b>	<b>0.93</b>

convolution. (5) “w/o Dual”: the dual learning strategy is removed, meaning that the loss is applied to only one frame in each iteration.

The results are summarized in Table 3. By comparing “w/o LR” with the full setting (“Full”), we can clearly demonstrate the effectiveness of our proposed constraint for the reflectance map. Similarly, the significant advantage of “Full” over “w/o LL” highlights the significance of the proposed illumination continuity constraint. Furthermore, we can validate the importance of mutually propagating features among different frames to achieve spatial-temporal consistent decomposition by comparing “w/o C.F.” with “Full”. Our proposed propagation strategy via the dual network structure proves to be more effective than the common method of using multi-frame inputs for propagation in videos, as seen in the comparison between “w/o M.I.” and “Full”. The dual learning setting, where we simultaneously supervise the two outputs of the dual network, also proves to be valuable, as evidenced by the comparison between “w/o Dual” and “Full”.

#### 4.5 User Study

To prove the effectiveness of our proposed framework in terms of human subjective evaluation, we conduct a large-scale user study with 100 participants with varying ages and education backgrounds, and balanced sex distribution. We aim to compare the perceptual quality of our method against SOTA baselines. To conduct the user study, we randomly collect 30 videos in the wild with the capture device of Sony A7R3 and iPhone13 (all models in the user study are trained with DID, since it is a large-scale dataset with multiple scenes and devices). Following most of the existing low-light enhancement works Xu et al. [2023b], Wang et al. [2023a], we employ the AB-test for the user study. For a video, the result produced by our method is called “Video A” whereas the result from another baseline is “Video B”. During the evaluation, each participant will compare the results of our method against other baselines in random order. For the comparison with one baseline, 5 videos will be randomly selected for visual perception. Each participant would simultaneously watch videos A and B. To avoid the bias caused by the position, we will randomize the left-right presentation order when showing videos A and B in each question. The participants can choose among three options: “Video A is better”, “Video B is better”, and “I think they are of the same quality”. They should make the decision according to the natural brightness, contrast, and color of each frame; the rich details, fewer artifacts, and the temporal consistency in the video. For each participant, the number of tasks is 10 methods  $\times$  5 videos = 50, and it took around 50 minutes on average for each participant to complete the user study.

Fig. 7 summarizes the user study’s results, and we can see that ours gets more selections from participants over all the baselines. This demonstrates that our method’s results are more preferred by the human subjective perception.

Table 4: Quantitative comparison on 3D low-light datasets with normal-light pairs, proposed in Wang et al. [2023a].

Methods	PairLLE	SNR	RetinexFormer	SCI+NeRF	Ours
PSNR	18.35	18.87	19.49	13.08	<b>21.09</b>
SSIM	0.604	0.650	0.702	0.505	<b>0.763</b>
Methods	PairLLE+NeRF	SNR+NeRF	RetinexFormer+NeRF	LLNeRF	Ours+NeRF
PSNR	18.72	19.24	19.98	20.50	<b>22.35</b>
SSIM	0.681	0.693	0.736	0.758	<b>0.782</b>

#### 4.6 Enhancement for NeRF

Recent works have introduced the implementation of 3D low-light enhancement Wang et al. [2023a], with a primary focus on disentangling view-independent intrinsic color and view-varying illuminations to achieve 3D-consistent enhancement. On the other hand, our framework’s enhanced results are particularly well-suited for NeRF reconstruction, as we have implemented a decomposition that maintains consistency across different spatial locations within a 3D scene.

To assess the impact of using our enhanced results for NeRF, we conducted experiments on a multi-view low-light dataset previously introduced in Wang et al. [2023a]. We employed the network trained on DID, as it benefits from a large-scale training dataset, resulting in solid generalization capabilities. Furthermore, DID inherently contains multi-view images. Specifically, for each view, we selected its closest view as the reference view for our input data.

In Table 4, we present the PSNR and SSIM results on the testing set of Wang et al. [2023a], where ground truth data is available. It’s important to note that none of the networks were fine-tuned on the testing set. The superiority of our framework is evident, as our network can achieve 3D-consistent enhancement that aligns with the fundamental principles of NeRF.

## 5 Conclusion

We introduce a novel LLVE framework that utilizes spatial-temporal consistent illumination and reflection decomposition and dual networks for mutual feature propagation. It predicts the decomposition of normal-light outputs without external priors, thanks to cross-frame correspondences and practical illumination continuity. Extensive experiments on various datasets showcase the framework’s superiority over SOTA approaches and the impact of our designed components.

## References

- Bolun Cai, Xianming Xu, Kailing Guo, Kui Jia, Bin Hu, and Dacheng Tao. A joint intrinsic-extrinsic prior model for Retinex. In *ICCV*, 2017.
- Jianrui Cai, Shuhang Gu, and Lei Zhang. Learning a deep single image contrast enhancer from multi-exposure images. *IEEE TIP*, 2018.
- Yuanhao Cai, Hao Bian, Jing Lin, Haoqian Wang, Radu Timofte, and Yulun Zhang. Retinexformer: One-stage retinex-based transformer for low-light image enhancement. In *ICCV*, 2023.
- Chen Chen, Qifeng Chen, Minh N. Do, and Vladlen Koltun. Seeing motion in the dark. In *ICCV*, 2019.
- Shivam Chhrirolya, Sameer Malik, and Rajiv Soundararajan. Low light video enhancement by learning on static videos with cross-frame attention. In *BMVC*, 2022.
- Johan Edstedt, Ioannis Athanasiadis, Mårten Wadenbäck, and Michael Felsberg. Dkm: Dense kernelized feature matching for geometry estimation. In *CVPR*, 2023.
- Huiyuan Fu, Wenkai Zheng, Xicong Wang, Jiakuan Wang, Heng Zhang, and Huadong Ma. Dancing in the dark: A benchmark towards general low-light video enhancement. In *ICCV*, 2023a.
- Zhenqi Fu, Yan Yang, Xiaotong Tu, Yue Huang, Xinghao Ding, and Kai-Kuang Ma. Learning a simple low-light image enhancer from paired low-light instances. In *CVPR*, 2023b.
- Samuel W. Hasinoff, Dillon Sharlet, Ryan Geiss, Andrew Adams, Barron Jonathan T., Florian Kainz, Jiawen Chen, and Marc Levoy. Burst photography for high dynamic range and low-light imaging on mobile cameras. *ACM Transactions on Graphics (Proc. SIGGRAPH Asia)*, 2016.

- Andrey Ignatov, Nikolay Kobyshev, Radu Timofte, Kenneth Vanhoey, and Luc Van Gool. DSLR-quality photos on mobile devices with deep convolutional networks. In *ICCV*, 2017.
- Haiyang Jiang and Yinqiang Zheng. Learning to see moving objects in the dark. In *ICCV*, 2019.
- Yifan Jiang, Xinyu Gong, Ding Liu, Yu Cheng, Chen Fang, Xiaohui Shen, Jianchao Yang, Pan Zhou, and Zhangyang Wang. EnlightenGAN: Deep light enhancement without paired supervision. *IEEE TIP*, 2021.
- Hanul Kim, Su-Min Choi, Chang-Su Kim, and Yeong Jun Koh. Representative color transform for image enhancement. In *ICCV*, 2021.
- Edwin H. Land. The Retinex theory of color vision. *Scientific American*, 1977.
- Edwin H Land and John J McCann. Lightness and retinex theory. *Josa*, 1971.
- Mading Li, Jiaying Liu, Wenhan Yang, Xiaoyan Sun, and Zongming Guo. Structure-revealing low-light image enhancement via robust Retinex model. *IEEE TIP*, 2018.
- Jinxu Liang, Yixin Yang, Boyu Li, Peiqi Duan, Yong Xu, and Boxin Shi. Coherent event guided low-light video enhancement. In *ICCV*, 2023.
- Lin Liu, Junfeng An, Jianzhuang Liu, Shanxin Yuan, Xiangyu Chen, Wengang Zhou, Houqiang Li, Yan Feng Wang, and Qi Tian. Low-light video enhancement with synthetic event guidance. In *AAAI*, 2023.
- Risheng Liu, Long Ma, Jiaao Zhang, Xin Fan, and Zhongxuan Luo. Retinex-inspired unrolling with cooperative prior architecture search for low-light image enhancement. In *CVPR*, 2021.
- Kin Gwn Lore, Adedotun Akintayo, and Soumik Sarkar. LLNet: A deep autoencoder approach to natural low-light image enhancement. *PR*, 2017.
- Feifan Lv, Feng Lu, Jianhua Wu, and Chongsoon Lim. MBLEN: Low-light image/video enhancement using CNNs. In *BMVC*, 2018.
- Xiaoqian Lv, Shengping Zhang, Chenyang Wang, Weigang Zhang, Hongxun Yao, and Qingming Huang. Unsupervised low-light video enhancement with spatial-temporal co-attention transformer. *TIP*, 2023.
- Long Ma, Tengyu Ma, Risheng Liu, Xin Fan, and Zhongxuan Luo. Toward fast, flexible, and robust low-light image enhancement. In *CVPR*, 2022.
- Jordi Pont-Tuset, Federico Perazzi, Sergi Caelles, Pablo Arbeláez, Alex Sorkine-Hornung, and Luc Van Gool. The 2017 davis challenge on video object segmentation. *arXiv*, 2017.
- Olaf Ronneberger, Philipp Fischer, and Thomas Brox. U-net: Convolutional networks for biomedical image segmentation. In *International Conference on Medical image computing and computer-assisted intervention*, 2015.
- Danai Triantafyllidou, Sean Moran, Steven McDonagh, Sarah Parisot, and Gregory Slabaugh. Low light video enhancement using synthetic data produced with an intermediate domain mapping. In *ECCV*, 2020.
- Ashish Vaswani, Noam Shazeer, Niki Parmar, Jakob Uszkoreit, Llion Jones, Aidan N. Gomez, Łukasz Kaiser, and Illia Polosukhin. Attention is all you need. In *NeurIPS*, 2017.
- Haoyuan Wang, Xiaogang Xu, Ke Xu, and Rynson WH Lau. Lighting up nerf via unsupervised decomposition and enhancement. In *ICCV*, 2023a.
- Qianqian Wang, Yen-Yu Chang, Ruojin Cai, Zhengqi Li, Bharath Hariharan, Aleksander Holynski, and Noah Snavely. Tracking everything everywhere all at once. In *ICCV*, 2023b.
- Ruixing Wang, Qing Zhang, Chi-Wing Fu, Xiaoyong Shen, Wei-Shi Zheng, and Jiaya Jia. Underexposed photo enhancement using deep illumination estimation. In *CVPR*, 2019a.

- Ruixing Wang, Xiaogang Xu, Chi-Wing Fu, Jiangbo Lu, Bei Yu, and Jiaya Jia. Seeing dynamic scene in the dark: High-quality video dataset with mechatronic alignment. In *ICCV*, 2021a.
- Tao Wang, Yong Li, Jingyang Peng, Yipeng Ma, Xian Wang, Fenglong Song, and Youliang Yan. Real-time image enhancer via learnable spatial-aware 3D lookup tables. In *ICCV*, 2021b.
- Wei Wang, Xin Chen, Cheng Yang, Xiang Li, Xuemei Hu, and Tao Yue. Enhancing low light videos by exploring high sensitivity camera noise. In *ICCV*, 2019b.
- Wenjing Wang, Xinhao Wang, Wenhan Yang, and Jiaying Liu. Unsupervised face detection in the dark. *IEEE TPAMI*, 2022a.
- Yufei Wang, Renjie Wan, Wenhan Yang, Haoliang Li, Lap-Pui Chau, and Alex Kot. Low-light image enhancement with normalizing flow. In *AAAI*, 2022b.
- Chen Wei, Wenjing Wang, Wenhan Yang, and Jiaying Liu. Deep Retinex decomposition for low-light enhancement. In *BMVC*, 2018.
- Wenhui Wu, Jian Weng, Pingping Zhang, Xu Wang, Wenhan Yang, and Jianmin Jiang. URetinex-Net: Retinex-Based deep unfolding network for low-light image enhancement. In *CVPR*, 2022a.
- Yirui Wu, Haifeng Guo, Chinmay Chakraborty, Mohammad Khosravi, Stefano Berretti, and Shaohua Wan. Edge computing driven low-light image dynamic enhancement for object detection. *IEEE Transactions on Network Science and Engineering*, 2022b.
- Ke Xu, Xin Yang, Baocai Yin, and Rynson WH. Lau. Learning to restore low-light images via decomposition-and-enhancement. In *CVPR*, 2020.
- Xiaogang Xu, Ruixing Wang, Chi-Wing Fu, and Jiaya Jia. SNR-Aware low-light image enhancement. In *CVPR*, 2022.
- Xiaogang Xu, Ruixing Wang, Chi-Wing Fu, and Jiaya Jia. Deep parametric 3d filters for joint video denoising and illumination enhancement in video super resolution. In *AAAI*, 2023a.
- Xiaogang Xu, Ruixing Wang, and Jiangbo Lu. Low-light image enhancement via structure modeling and guidance. In *CVPR*, 2023b.
- Jianzhou Yan, Stephen Lin, Bing Kang Sing, and Xiaoou Tang. A learning-to-rank approach for image color enhancement. In *CVPR*, 2014.
- Zhicheng Yan, Hao Zhang, Baoyuan Wang, Sylvain Paris, and Yizhou Yu. Automatic photo adjustment using deep neural networks. *ACM TOG*, 2016.
- Wenhan Yang, Shiqi Wang, Yuming Fang, Yue Wang, and Jiaying Liu. Band representation-based semi-supervised low-light image enhancement: Bridging the gap between signal fidelity and perceptual quality. *IEEE TIP*, 2021a.
- Wenhan Yang, Wenjing Wang, Haofeng Huang, Shiqi Wang, and Jiaying Liu. Sparse gradient regularized deep Retinex network for robust low-light image enhancement. *IEEE TIP*, 2021b.
- Jing Ye, Changzhen Qiu, and Zhiyong Zhang. Spatio-temporal propagation and reconstruction for low-light video enhancement. *Digital Signal Processing*, 2023.
- Syed Waqas Zamir, Aditya Arora, Salman Khan, Munawar Hayat, Fahad Shahbaz Khan, Ming-Hsuan Yang, and Ling Shao. Learning enriched features for real image restoration and enhancement. In *ECCV*, 2020.
- Hui Zeng, Jianrui Cai, Lida Li, Zisheng Cao, and Lei Zhang. Learning image-adaptive 3D lookup tables for high performance photo enhancement in real-time. *IEEE TPAMI*, 2020.
- Fan Zhang, Yu Li, Shaodi You, and Ying Fu. Learning temporal consistency for low light video enhancement from single images. In *CVPR*, 2021.
- Yonghua Zhang, Jiawan Zhang, and Xiaojie Guo. Kindling the darkness: A practical low-light image enhancer. In *ACM MM*, 2019.

Lin Zhao, Shao-Ping Lu, Tao Chen, Zhenglu Yang, and Ariel Shamir. Deep symmetric network for underexposed image enhancement with recurrent attentional learning. In *ICCV*, 2021.

Chuanjun Zheng, Daming Shi, and Wentian Shi. Adaptive unfolding total variation network for low-light image enhancement. In *ICCV*, 2021.